Planetary and Space Science 259 (2025) 106061

Contents lists available at ScienceDirect

Planetary and Space Science

journal homepage: www.elsevier.com/locate/pss

The refractory-to-ice ratio in comet 67P: Implications on the composition of the comet-forming region of the protoplanetary disk

Raphael Marschall [a,*], Alessandro Morbidelli [b], Yves Marrocchi [c]

[a] CNRS, Observatoire de la Côte d'Azur, Laboratoire J.-L. Lagrange, CS 34229, Nice Cedex 4, 06304, France
[b] College de France, Centre National de la Recherche Scientifique, Université Paris Sciences et Lettres, Sorbonne Université, Paris, 75014, France
[c] Université de Lorraine, CNRS, CRPG, UMR 7358, Nancy, 54000, France

ARTICLE INFO

Keywords:
Comets
67P/Churyumov–Gerasimenko
Elemental composition
Formation location
Protoplanetary disk

ABSTRACT

Comets, asteroids, and other small bodies are thought to be remnants of the original planetesimal population of the Solar System. As such, their physical, chemical, and isotopic properties hold crucial details on how and where they formed and how they evolved. Yet, placing precise constraints on the formation region of these bodies has been challenging. Data from spacecraft missions have a particularly high potential of addressing the question of the origin of the visited bodies. ESA's Rosetta mission to comet 67P/Churyumov-Gerasimenko returned data from the comet for two years on its journey around the Sun. This extensive data set has revolutionized our view on comets and still holds unsolved problems.

Here, we aim to determine comet 67P's bulk elemental composition from Rosetta data, including its refractory-to-ice ratio. We use these results to constrain the temperature in the protoplanetary disk where comets formed and, using a disk model, the formation location.

We use the Rosetta/ROSINA (Rosetta Orbiter Spectrometer for Ion and Neutral Analysis) measurement of the volatile/ice composition and the Rosetta/COSIMA (COmetary Secondary Ion Mass Analyzer) measurements of the refractory composition of comet 67P. These measurements are combined using a Monte Carlo method. The refractory-to-ice ratio is a free parameter that is constrained a posteriori.

Using only the composition, we constrain the refractory-to-ice ratio to $0.5 < \chi < 1.7$, and derive the bulk elemental abundances for 67P of H, C, N, O, Na, Mg, Al, S, K, Ar, Ca, Cr, Mn, Fe, Kr, and Xe. We find the noble gas xenon in near solar elemental abundance in comet 67P. Krypton is slightly depleted, while argon is heavily depleted. Comet 67P is enriched in all three noble gases by up to 2.5 orders of magnitude compared to CI chondrites. We show this is consistent with a formation region between 25 and 35 au in a protoplanetary disk region with temperatures between 30 and 40 K and with the trapping of dust for a long time in rings of the protoplanetary disk.

1. Introduction

It is commonly argued that studying small Solar System bodies (asteroids, comets, etc.) directly informs planet formation theories because they are remnants of the original planetesimal population that triggered Solar System formation. Comets are considered among the most pristine objects in our Solar System because their physical and chemical properties are most easily explained by a lack of internal processing. For example, comets have very low densities (~500 kg m^{-3}; Groussin et al., 2019) and contain significant amounts of highly-volatile ices (incl. CO and CO_2; Eberhardt et al., 1987; Gasc et al., 2017). Although most comets have typical diameters between 1-5 km (Snodgrass et al., 2011), the mentioned properties appear to hold even for large comets (e.g., Biver et al., 1997; Kelley et al., 2022; Spencer et al., 2020; Brown, 2013), suggesting that these bodies experienced minimal heating or other planetary processes. This view that comets are, to a large extent, primordial is consistent with our current understanding of their dynamical past. They have presumably formed beyond Neptune in a massive primordial disk of precursory bodies, commonly referred to as planetesimals or cometesimals (e.g. Nesvorný, 2018, for a review of the dynamics in the early Solar System). When Neptune migrated through that disk, these bodies were scattered into the current day Kuiper Belt – in particular, the so-called Scattered Disk – where they have remained until recently (e.g. Nesvorný et al., 2016; Nesvorný, 2021). The Scattered Disk is widely considered as the main source reservoir of Jupiter family comets (JFC; Duncan et al., 2004; Duncan, 2008; Dones et al., 2015). From the Scattered Disk, comets are injected

* Corresponding author.
E-mail address: raphael.marschall@oca.eu (R. Marschall).

https://doi.org/10.1016/j.pss.2025.106061
Received 3 September 2024; Received in revised form 20 January 2025; Accepted 27 January 2025
Available online 18 February 2025

into the inner Solar System by the giant planets. Once close enough to the Sun, they exhibit activity driven by the sublimation of ices (in particular H_2O).

Because JFCs can have very low perihelia (~1 au), they are also the most easily accessible comet population for interplanetary spacecraft. Over the past three decades, they have thus become the target of multiple international missions, including 19P/Borrelly (Deep Space 1, Rayman, 2002), 81P/Wild 2 (Stardust, Reichhardt, 1995), 9P/Tempel 1 (Stardust, and Deep Impact, A'Hearn et al., 2005), 103P/Hartley 2 (Deep Impact/EPOXI, A'Hearn et al., 2011), and most recently 67P/Churyumov-Gerasimeko (Rosetta, Taylor et al., 2017).

Rosetta was the first mission to go into orbit around a comet. Two years at 67P/Churyumov-Gerasimenko (hereafter 67P) gave us an unprecedented up-close look at the physical and chemical properties as well as the evolution of 67P along its orbit from 3.7 au on the inbound orbit to perihelion at 1.25 au and back out to 3.8 au. Rosetta has revolutionized our understanding of comets (see Keller and Kührt, 2020, for a review). Yet many questions remain open. In particular, the hope that we can determine how comets formed has not been fulfilled. Proponents of conflicting formation scenarios have claimed Rosetta's observations confirm their theories (see Weissman et al., 2020).

One main objective, finding the formation location of comet 67P, has not yet been addressed, and it is one of our goals. In this work, we combine measurements from two analytical instruments from the Rosetta space mission: (i) "Rosetta Orbiter Spectrometer for Ion and Neutral Analysis" (ROSINA) and (ii) "COmetary Secondary Ion Mass Analyzer" (COSIMA) instruments to deduce the bulk chemical composition of 67P. We will show that the noble gas xenon is present in solar abundance, which strongly suggests that it has been accreted in solid form, while argon was accreted out of the gas phase. Krypton being slightly depleted is suggestive that the comet formed close, but slightly inward, of the krypton sublimation line. This implies the formation of comet 67P and JFCs, more generally, at roughly 25–35 au in the protoplanetary disk. This constraint is solely driven by composition but is consistent with dynamical models on the origin and evolution of Jupiter family comets.

2. Deriving the bulk composition of comet 67P

The bulk elemental abundance of 67P was not measured directly. Instead, two instruments measured two different components, which we call here the ice (anything measured as a gas in the coma) and refractory (measured on solid dust particles) components. The ice component was measured by the Rosetta Orbiter Spectrometer for Ion and Neutral Analysis (ROSINA; Balsiger et al., 2007). The refractory component was measured on dust particles collected by the COmetary Secondary Ion Mass Analyzer (COSIMA; Kissel et al., 2007).

To get the bulk elemental composition of 67P, we need to combine these two components. To do so and to properly track the errors and uncertainties, we model the data from both ROSINA and COSIMA, assuming that the respective measured values represent the median of a log-normal distribution and the respective errors are 1-σ errors. Taking one million random draws of each element with the respective distribution gives a good match to the data, as shown in the (Fig. 6).

2.1. The refractory component from COSIMA

The COSIMA instrument collected dust particles in the coma of 67P. These particles were, amongst other things, analyzed with a high-resolution time-of-flight secondary ion mass spectrometer. The elemental abundances of the cometary dust that we are using here were presented in Table 3 of Bardyn et al. (2017). The Nitrogen to carbon ratio, N/C, was measured by Fray et al. (2017).

Here, we use all the elemental abundances with respect to iron, Fe. But, because N/Fe was not directly measured the 'minus'-error became very large when deriving it from the measurements of the N/C, C/Si, and Si/Fe ratios. Because this large error leads to a negative lower bound for the N/Fe ratio, which is non-physical, we have chosen to use the logarithm of the 'positive' error also for the 'negative' error. This, in principle, can overestimate the abundance of Nitrogen, but given that Nitrogen is almost two orders of magnitude depleted with respect to the major elements of hydrogen, carbon, and oxygen, we believe this assumption is justified and will not affect our results in a significant way.

Another assumption of the COSIMA measurements is that the hydrogen-to-carbon atomic ratio is 1.04 ± 0.16 (Isnard et al., 2019). This is justified by the fact that the macro-molecules that were detected in 67Ps particles contain more H than the Insoluble Organic Matter (IOM) measured in chondritic meteorites (Fray et al., 2016). The highest H/C in IOM that was measured is 0.8 (Alexander et al., 2007). We thus adopt this same assumption as Isnard et al. (2019) and Bardyn et al. (2017). Additionally, COSIMA found that the refractory component of 67P is made up by roughly one half in organics and the other half in minerals. All used measurements from Bardyn et al. (2017) and Fray et al. (2017), as well as the log-normal parameters used to model the measurements, are listed in Table 1.

To zeroth order, the refractory component of 67P consists of equal parts of hydrogen, carbon, and oxygen (left panel of Fig. 6). The next most abundant element, silicon, is a factor of four less abundant than the three major elements. All other species are at least 1.5 orders of magnitude less abundant than the major elements. Potassium is the least abundant of the measured elements and is depleted by more than three orders of magnitude compared to hydrogen.

2.2. The ice component from ROSINA

The composition of the gases in the coma of 67P was measured by the ROSINA instrument. ROSINA consisted of three subsystems: the Double-Focusing Mass Spectrometer (DFMS), the Reflectron-type Time-Of-Flight mass spectrometer (RTOF), and the Comet Pressure Sensor (COPS). Rubin et al. (2019) determined the molecular abundances of 45 major and minor volatile species with respect to water. We use these values to derive the elemental abundances with respect to water (right panel of Fig. 6). Table 2 lists the ROSINA measurements and the log-normal parameters used to model the measurements.

Compared to the refractory component, the volatiles are depleted in carbon. Hydrogen and oxygen are still the major elements, while sulfur and nitrogen are both less abundant by two orders of magnitude, similar to the refractory component. The three noble gases argon, krypton, and xenon are five to seven orders of magnitude less abundant than hydrogen.

2.3. Constraining the refractory-to-ice mass ratio

To combine the refractory and volatile/ice components and arrive at the bulk elemental composition of 67P, we are left with one unknown: the refractory-to-ice mass ratio, χ. There is considerable debate on the value of χ for 67P, or any comet for that matter (see review by Choukroun et al., 2020). Values from 0.1 to 10 and higher can be found in the literature. The large discrepancies in these values result primarily from a lack of knowledge about how much dust falls back to the surface and to what extent that dust has lost its ice component while on ballistic trajectories around the comet.

Rubin et al. (2019) derived bulk elemental abundances for hydrogen, carbon, oxygen, nitrogen, and silicon, assuming χ equal to one and three. Here, we take a different approach and start by being agnostic about the value of χ and thus initially leave it as a free parameter. We will see later that doing that will allow us to independently constrain χ using only arguments of the elemental composition. Additionally, we derive the bulk elemental abundances for 12 additional elements (Na, Mg, Al, S, K, Ar, Ca, Cr, Mn, Fe, Kr, Xe), which crucially also includes the noble gases argon, krypton, and xenon.

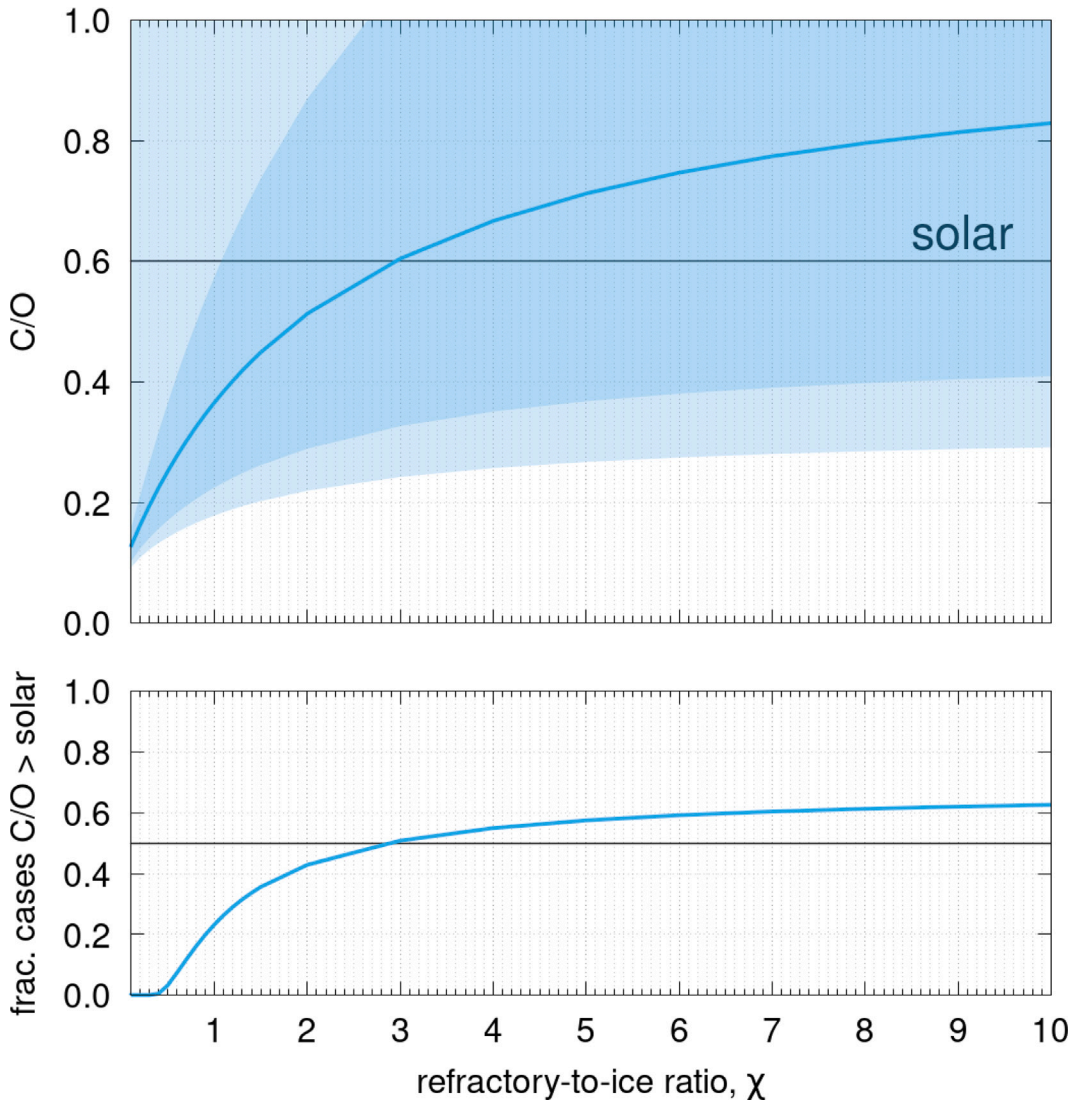

Fig. 1. The top panel shows the bulk carbon-to-oxygen atomic ratio of comet 67P as a function of the refractory-to-ice mass ratio, χ. The dark blue shaded area encompasses 50% of the cases, and the light blue $\pm 1\sigma$. The solar value of 0.594 is taken from Asplund et al. (2021). The bottom panel shows the fraction of cases with a super-solar C/O ratio.

Thus, for each value of χ, we draw a random composition for the refractory and volatile/ice components, assuming the log-normal distribution described above. Each component is mixed with the other at the respective χ, from which we can calculate the resulting bulk elemental composition. By performing one million such random draws, we can calculate the median elemental composition and the associated 1-σ errors.

Fig. 1 shows the resulting carbon-to-oxygen ratio as a function of χ. The dark blue shaded area encompasses 50% of the cases, and the light blue $\pm 1\sigma$. The error bars are large and become larger as χ increases because of the large uncertainties of the C and O abundances of the refractory component.

It would be reasonable to assume that the C/O ratio could be as high as the solar value (Asplund et al., 2021) but should not be super-solar. In the median case, this is true up to $\chi = 3$. The bottom panel of Fig. 1 show the fraction of cases with a super-solar C/O ratio. It shows that even at high χ there are still roughly 40% of cases where 67P would have a sub-solar C/O ratio. This might be acceptable to some, but we would posit that if the condition of having a sub-solar C/O ratio is strongly weighted, that would clearly point in the direction of smaller χ. For example at a $\chi = 1$ almost 80% of cases would be sub-solar. Nevertheless, the C/O ratio, though pointing towards small χ, is not a strong constraint on χ.

Therefore, we will have a look next at the oxygen composition as a function of χ. This is particularly interesting because we can split the oxygen into a part that is stored in water (O_{ex}) and the one that is stored in anhydrous material (O_{an}). This is analogous to what has been done for meteorites (Alexander, 2019), e.g., the primitive CI chondrites. Fig. 2 shows the oxygen composition of 67P and its comparison to CI chondrites. The anhydrous oxygen composition compared to silicon is independent of χ because it is simply the composition of the refractory component. But the amount of oxygen in water (with respect to silicon) decreases with increasing χ because the fraction of water decreases with increasing χ.

In the median case, if $\chi = 1.7$, the ratio between the abundance of oxygen in water and anhydrous minerals is the same as in CI chondrites (Fig. 2). This case already seems unusual, as we might expect a comet to have more oxygen in water than a carbonaceous chondrite. The comet is non-chondritic if $\chi < 1.1$. Nevertheless, we consider the $\chi = 1.7$ case ("chondritic" case) the upper limit. Remember that for $\chi < 3$, the median C/O ratio is also always sub-solar and therefore, for $\chi < 1.7$, most cases will result in a sub-solar C/O ratio.

To summarize this part: When starting with an agnostic stance on what the refractory-to-ice mass ratio, χ, for 67P should be, from the elemental composition alone constrains $\chi < 1.7$. This is lower than what was found very early in the mission ($\chi = 4 \pm 2$; Rotundi et al., 2015) but

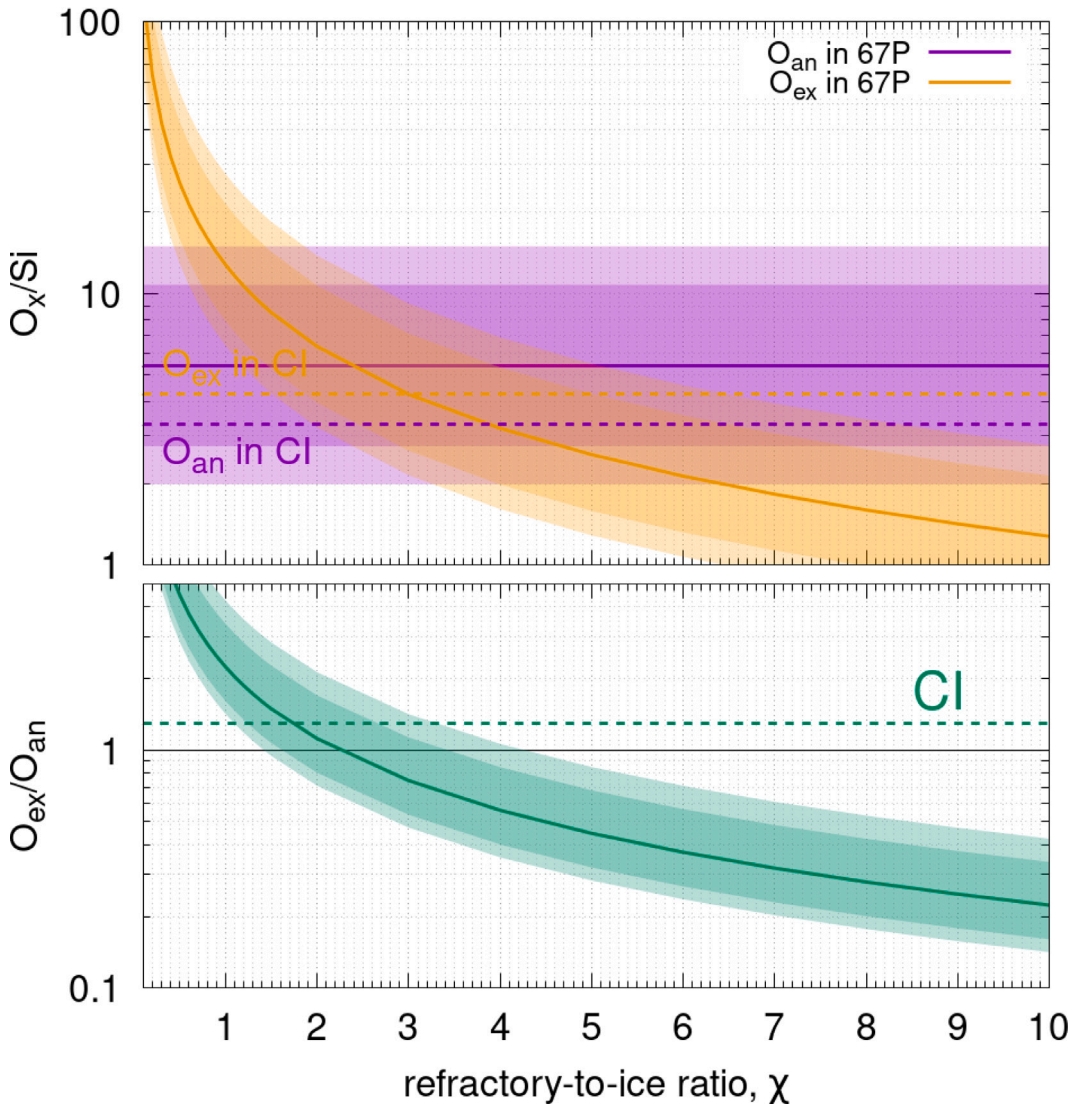

Fig. 2. The top panel shows the oxygen-to-silicon ratio for oxygen that is in water (subscript 'ex') and that which is in anhydrous form (subscript 'an'). The values for CI chondrites are taken from Alexander (2019). The bottom panel shows the ratio of the two oxygen components. Note that the bottom panel is not simply the ratio of the lines in the top panel. O_{ex} and O_{an} are not uncorrelated, and therefore, their ratio and respective errors need to be computed for each random draw. The darker shaded areas contain 50% of the cases while the lighter areas contain $\pm 1\sigma$.

in line with measurements from the coma of 67P (Biver et al., 2019; Marschall et al., 2020b; Läuter et al., 2020; Combi et al., 2020). Initially, there was a significant discrepancy between the estimates for the gas production rates derived from remote sensing (e.g., the MIRO and VIRTIS instrument) and in-situ measurements (ROSINA). Later studies resolved this, and now the different estimates are in line with each other (Biver et al., 2019; Combi et al., 2020). Furthermore, Marschall et al. (2020b) showed that the refractory-to-ice ratio is variable during the mission. It was highest very early on in the mission (~1.6) when the value of Rotundi et al. (2015) was measured. Between perihelion and summer solstice, when the production rates were the highest and thus the time most representative of the bulk mass loss, the refractory-to-ice ratio dropped to ~0.5. The similarity between the values we find here and the ones measured in the coma (Biver et al., 2019; Marschall et al., 2020b; Läuter et al., 2020; Combi et al., 2020) suggests that the material falling back to the surface is not significantly different from that of the bulk comet, i.e., it did not lose a significant part of its ice component while in the coma. This is in line with thermophysical models of fallback material, arguing for the retention of a significant amount of ices even for small cm-sized particles (Davidsson et al., 2021). Though we only discussed an upper limit for χ here, we will discuss a lower limit in the next section.

2.4. The bulk composition of 67P

Given the arguments above, we have constrained the refractory-to-ice mass ratio to $\chi < 1.7$. Fig. 3 presents an overview of the bulk abundances for 67P relative to the solar values for three different values of χ. The full list of values presented in that figure can be found in Tables 3 and 4.

Several things are of note. First, if $\chi < 0.3$ xenon becomes super-solar in 84% of the cases. There is no particular reason that xenon should be super-solar, so we can consider this a mild lower limit on χ.

Second, oxygen is super solar if $\chi < 0.5$ and becomes consistent with the solar value at $\chi \sim 0.5$. Thus, a rather plausible range for χ is $0.5 < \chi < 1.7$. For this range of χ the bulk mass fraction of water is between 28% ($\chi = 1.7$) to 52% ($\chi = 0.5$). Interestingly, the prediction from Bitsch and Battistini (2020) for a solar-type star is a water mass fraction of 35%. This is well within our range with a water mass fraction of 35% at $\chi = 1.2$. Oxygen is solar in the median case at $\chi = 1.1$ and thus represents our preferred case, which also happens to

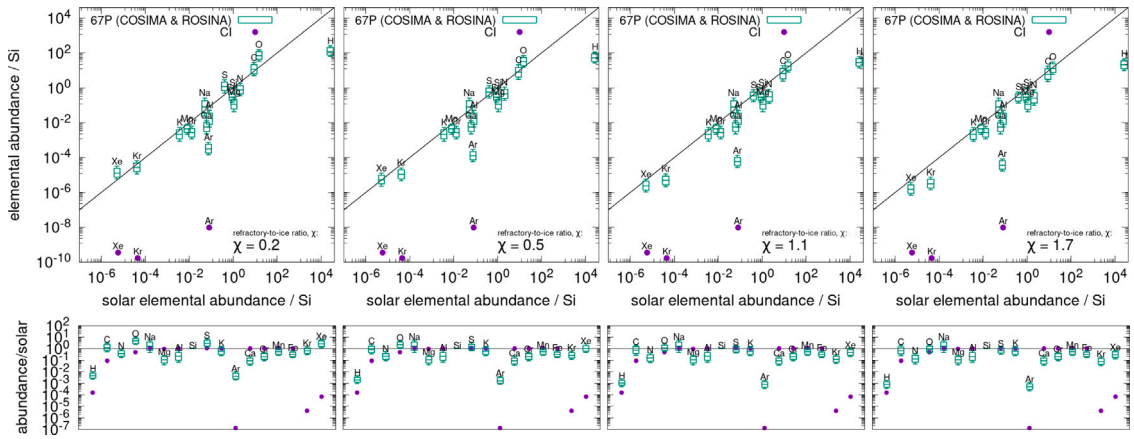

Fig. 3. The top panels of each column show the bulk elemental composition of 67P with respect to silicon compared to the solar elemental composition (Asplund et al., 2021). Each column shows the results for a different refractory-to-ice mass ratio, χ. The bottom panels of each column show the abundances of each element normalized to the solar values. The green boxes are the values for 67P, while the purple dots show the composition for CI chondrites (Alexander, 2019). All bulk abundances and corresponding errors for 67P are also available in Tables 3 and 4.

lie in the middle of our constraint of χ ($0.5 < \chi < 1.7$). Similarly, Bitsch and Battistini (2020) predict an oxygen mass fraction of 55% whereas we get a range of 58% ($\chi = 1.7$) to 69% ($\chi = 0.5$). An updated overview of literature values of χ for comet 67P can be found in the in Fig. 7.

Third, the noble gases argon, krypton, and xenon are all enriched by orders of magnitude compared to CI chondrites.

Fourth, and maybe most importantly, xenon (the least volatile of the three mentioned noble gases) is present in quasi solar abundance for all the plausible cases of χ (within 1σ xenon is solar for $\chi < 1.2$ and slightly sub-solar for larger χ). We can also look at Xe/H_2O for a sanity check, which comes only from the ROSINA measurements and does not rely on our modeling of the bulk abundances. For 67P, $Xe/H_2O = (2.4 \pm 1.1) \cdot 10^{-7}$ (Rubin et al., 2019) while for the Sun using the values by Lodders (2003) it is $(3.89 \pm 0.48) \cdot 10^{-7}$ [assuming all oxygen is in water], $(6.95 \pm 0.86) \cdot 10^{-7}$ [assuming 56% of the oxygen atoms are in water as in the case of our $\chi = 1.1$], and $(7.78 \pm 0.96) \cdot 10^{-7}$ [assuming half of the oxygen is in water]. The 67P xenon to water ratio is sub-solar by factors of 1.6 ± 0.8, 2.9 ± 1.4, and 3.2 ± 1.5 for the three cases assuming different amounts of oxygen trapped in water. Thus, even for the measurements only derived from ROSINA, xenon is quasi-solar.

Fifth, Krypton, which is slightly more volatile than xenon, is slightly depleted (factor of 3–10) with respect to the solar value. Argon, on the other hand, the most volatile of the three noble gases, is strongly depleted (~3 orders of magnitude) with respect to the solar value.

3. Discussion

We focus our discussion on the elemental abundances of the noble gases (Fig. 3). Krypton is slightly depleted relative to xenon, and argon is heavily depleted relative to both krypton and xenon. The important new constraint we introduce here is that xenon is present in the comet in solar abundance and about four orders of magnitude more abundant than in CI chondrites.

Noble gases can either be adsorbed in gaseous form in ice, or they can condense on icy grains if the disk temperature is low enough. Adsorption can only ever be partial. It cannot explain the solar abundance of xenon in 67P nor the fact that the isotopic properties of xenon in the comet are radically different from those of the Sun or the atmosphere of Jupiter (Marty et al., 2017). Thus, we think that the data from 67P rule adsorption out for xenon.

Condensation of noble gases on grains can, in principle, explain solar abundance. Moreover, if at least part of the noble gases had been injected into the disk already in condensed form, they would have avoided isotopic equilibration with the gas and preserved a distinct isotopic composition. The condensation temperatures of noble gases on grains are given in Öberg and Wordsworth (2019): roughly 20 K for argon, 30 K for krypton, and 45 K for xenon. Explaining the depletion pattern in 67P, however, is not trivial. The reason is that once the original grains aggregate into pebbles, noble gases are not expected to sublimate at the corresponding temperatures. They remain trapped in the icy matrix and are desorbed only at specific temperatures, primarily during the transformation of CO_2 and H_2O ices (Ligterink et al., 2024). These transformations start at about 50–60 K and equally for all noble gases. Thus, in a scenario where grains drift towards the Sun from the outer disk, they would contain xenon, krypton and argon in solar abundance until they reach this temperature. According to this, any object formed in a region of the disk colder than 50–60 K should have all noble gases in solar abundance, while objects formed in warmer portions of the disk can start fractionating their elemental ratios. Nevertheless, at any temperature, the strong depletion of argon relative to krypton and xenon observed in 67P is difficult to understand (Ligterink et al., 2024), even more so considering our result that xenon is in solar abundance.

We propose to solve this conundrum taking into account that comets very likely formed late in the protoplanetary disk phase. In fact, comets and other related large icy small bodies such as Trojans and Kuiper-belt objects have very low densities (between 300 kg m^{-3} and 1500 kg m^{-3}; Groussin et al., 2019; Berthier et al., 2020; Spencer et al., 2020) and contain highly-volatile ices, in particular CO and CO_2 (Eberhardt et al., 1987; Gasc et al., 2017; Kelley et al., 2022), which suggests that comets have never been significantly heated or even differentiated. Thus, they must have formed late (Neumann et al., 2018) at a time when most of the short-lived radiogenic material has already decayed, i.e., several million years after the formation of the oldest solids (CAIs; Amelin et al., 2010; Connelly et al., 2012). At that time, dust should have been trapped in disk structures, rather than still drifting towards the star. Evidence for this comes from the ubiquitous observation of dust rings in protoplanetary disks (Andrews, 2020) and the ratio between the disk sizes in dust and gas does not seem to shrink over time (Najita and Bergin, 2018). The observed evolution of disk sizes over time is totally inconsistent with models where dust continuously drifts towards the star (Appelgren et al., 2020; Birnstiel, 2024), demonstrating the need for dust traps due to radial pressure bumps. It is, therefore, reasonable to envision that dust remains trapped in pressure bumps for millions of years until the conditions (i.e., the dust/gas ratio, which increases as gas is removed) become favorable for late cometesimal formation.

Over these long timescales, the noble gases, even if initially trapped in water or CO_2 ice in the pebble, have plenty of time to diffuse to the surface, of the pebble (Smith et al., 1997; Livingston et al., 2002; Ligterink et al., 2024). Once the volatiles have reached the

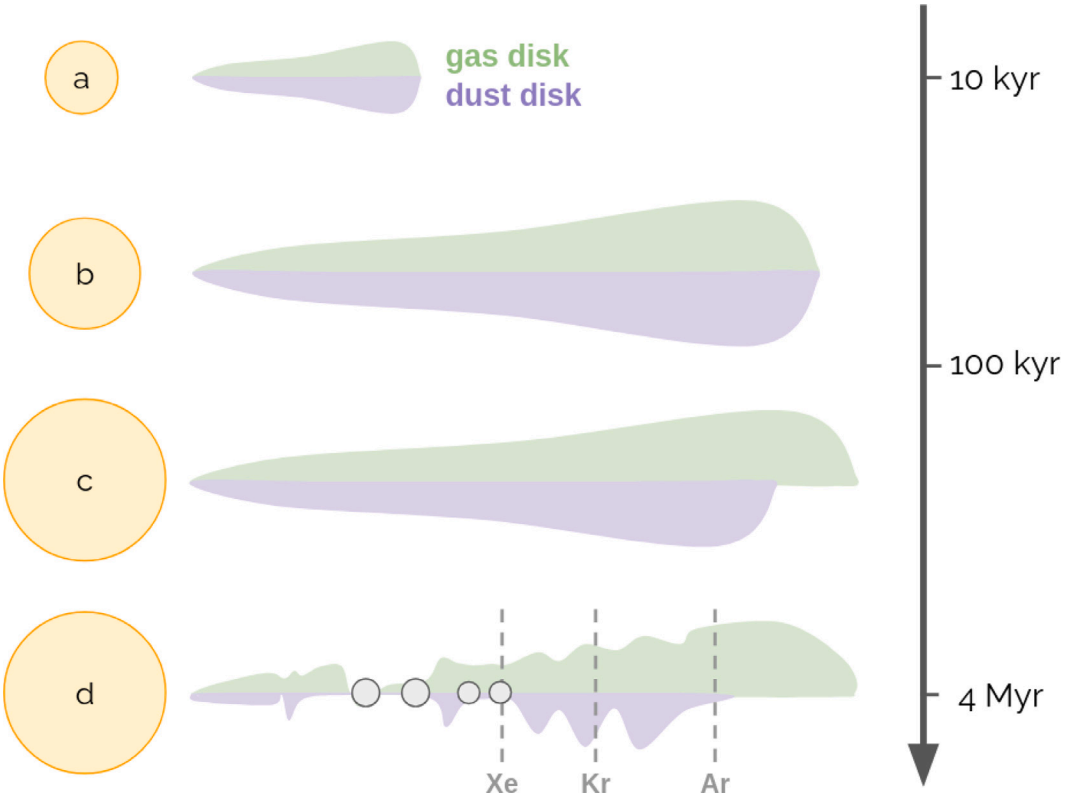

Fig. 4. A sketch of a protoplanetary disk scenario. Initially, the dust and gas disk expand together through the viscous expansion of the gas (e.g., Drążkowska and Dullemond, 2018; Morbidelli et al., 2022; Marschall and Morbidelli, 2023) (a & b). At some point, the dust grows large enough that radial inward drift due to aerodynamic drag in the tangential direction starts to dominate on short timescales (e.g., Takeuchi and Lin, 2002, 2005), and the dust disk begins to contract (c). Eventually, structures in the disk form Andrews (2020) and trap dust, thus preventing the complete loss of the dust disk (d). Dust pebbles trapped within these pressure bumps remain there until they are accreted into planetesimals. Depending on the location in the disk and the accretion time, pebbles lose volatiles/retain the respective volatile species. The xenon, krypton, and argon lines are illustrated as examples.

surface they can desorb/sublimate if the disk temperature is high enough, i.e. larger than the condensation/sublimation temperatures of Öberg and Wordsworth (2019). If a noble gas evaporates at the surface (e.g., argon), the diffusion continues, and over time the pebble becomes strongly depleted in that gas. If instead the temperature in the disk is too cold for evaporation of the noble gas at the surface of the pebble (e.g., xenon), diffusion stops and the pebble preserves its original abundance. Close but inwards of a sublimation line, we can envision that the process of diffusion and sublimation is slow, and in the end, the pebble is only partially depleted. This could be the case of krypton. This scenario is sketched in Fig. 4.

Fig. 5 shows the temperature profiles from our models of disks. The parameters of the model cover the same values as in Marschall and Morbidelli (2023) (e.g., in the assumed evolution of the disk viscosity). Here, in contrast to the results presented in Marschall and Morbidelli (2023), we explicitly consider the stellar radiation onto the disk when solving for the temperature. While the temperatures differ from model to model in the inner part of the disk, where viscous heating dominates, all of them show the same temperature profile beyond about 8 au. Beyond that distance, the temperature is dominated by stellar radiation and thus follows almost exactly what would be expected from the analytical solution for a passive disk (Chiang and Youdin, 2010).

The xenon line is at around 13 au, the krypton line is at roughly 45 au, and the one of argon is at 70 au. We argued above that 67P must have formed beyond the xenon line, thus beyond 13 au, to accrete xenon in solid form. 67P should not form too close to the xenon line, though, because, in this case, it would form in a xenon-enriched environment that would lead to super-solar abundances of xenon. Additionally, 67P also had to form close but still inside of the krypton line, i.e., inside of 35 au. How far inside of the krypton line 67P could have formed is unclear. But a reasonable guess would be that the formation region is somewhere in the 25–35 au region. This conclusion, obtained from compositional considerations, is well in line with the location of the reservoir of planetesimals that generated the scattered disk, the Oort cloud and the hot Kuiper belt population, according to dynamical models (Nesvorný, 2018), and thus with the dynamical origin of 67P.

Additionally, CI chondrites are depleted relative to comets by at least two orders of magnitude even when we assume a $\chi = 10$ (the order of magnitude for the amount of water in CIs; Fig. 3). In our scenario, this implies that CIs formed inside the xenon sublimation line, i.e., inside 12 au, namely the giant planet region. This distance is also consistent with dynamical models of CI formation beyond Jupiter and implantation into the asteroid belt (Raymond and Izidoro, 2017).

In our model, because the comet forms well inside the argon condensation line, the only argon present would be the one adsorbed from the protoplanetary disk. This is consistent with the results of Yokochi (2022), who showed experimentally that the adsorption of argon at 36–45 K (i.e. between the Kr and Xe lines) would lead to the observed Ar/H_2O ratio of 67P. Additionally, argon, adsorbed from the gas of the disk, would have solar isotopic composition, as observed (Balsiger et al., 2015). Both heating from solar radiation (e.g., Guilbert-Lepoutre et al., 2016; Gkotsinas et al., 2024) and collisions (e.g., Bottke et al., 2023; Jutzi and Michel, 2020) could further deplete argon.

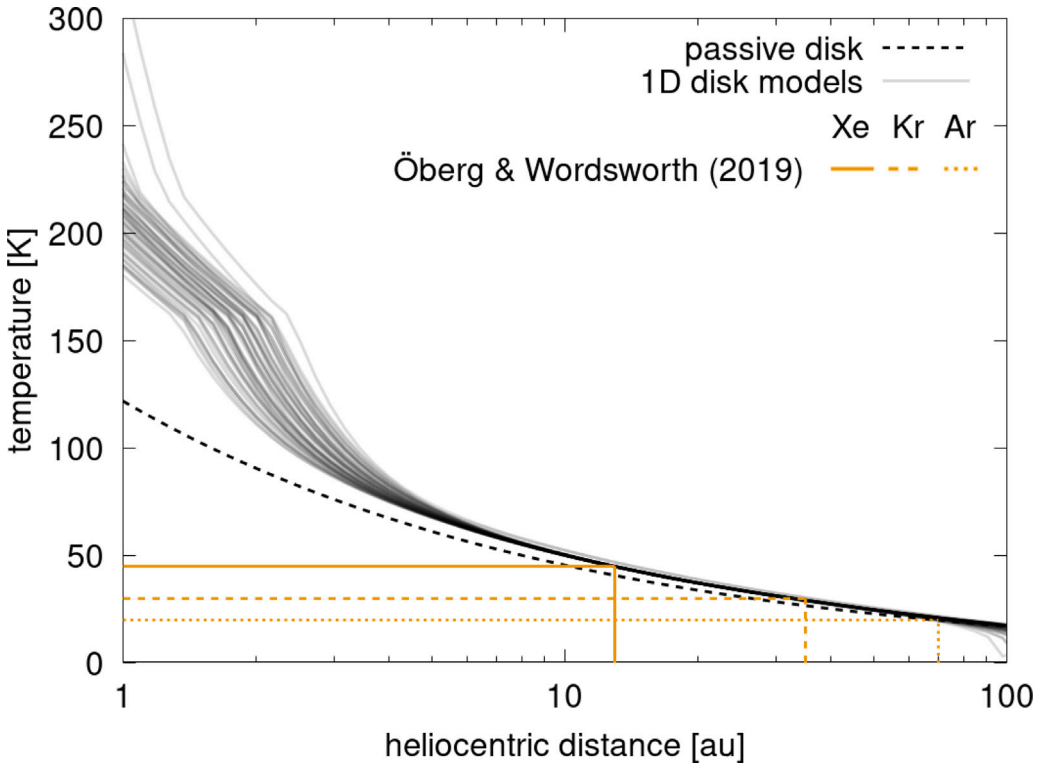

Fig. 5. The temperature as a function of heliocentric distance is shown for a large set of models of evolved protoplanetary disks (light grey lines). The black dashed line shows the temperature profile of a passive disk (Chiang and Youdin, 2010). The orange lines show the sublimation lines for xenon (solid), krypton (dashed), and argon (dotted) for the values presented in Öberg and Wordsworth (2019).

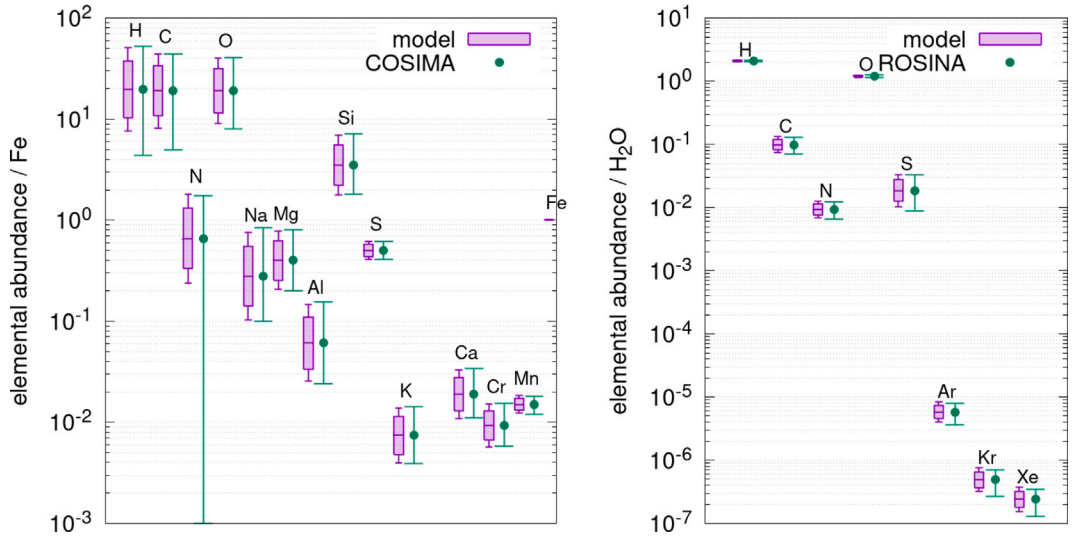

Fig. 6. The left panel shows the elemental abundances (number of atoms) of the refractory component with respect to iron, Fe, as measured by COSIMA, while the right panel shows the elemental abundances (number of atoms) of the volatile/ice component with respect to molecular water, H_2O, as measured by ROSINA. The green points represent the measurements of the respective instruments, and the purple box plots the results from the one million random draws from the respective log-normal distributions. The upper and lower bounds of the box contain 50% around the median while the whiskers contain 68%, i.e. $\pm 1\sigma$.

4. Conclusions

We have combined COSIMA and ROSINA data on the elemental abundances of comet 67P's refractory and volatile/ice components. To calculate the bulk elemental abundance of 67P, we started out being agnostic about the refractory-to-ice mass ratio, χ, and left it as a free parameter. The resulting elemental composition showed, though, that only $0.5 < \chi < 1.7$ leads to reasonable results. These constraints on χ come from the amount of oxygen in water vs. anhydrous material being not smaller than in CI chondrites as well as other elements (such as xenon and oxygen) not being in super-solar abundance relative to refractory elements. These values are consistent with other estimates from the coma of 67P (e.g. Biver et al., 2019; Marschall et al., 2020b; Läuter et al., 2020; Combi et al., 2020; Choukroun et al., 2020) and suggest little volatile loss from material falling back to the nucleus, which is also consistent with thermophysical studies of the fallback material (Davidsson et al., 2021). For these values of χ comet 67P would have a $0.2 < C/O < 0.4$. Furthermore, for the mentioned range in

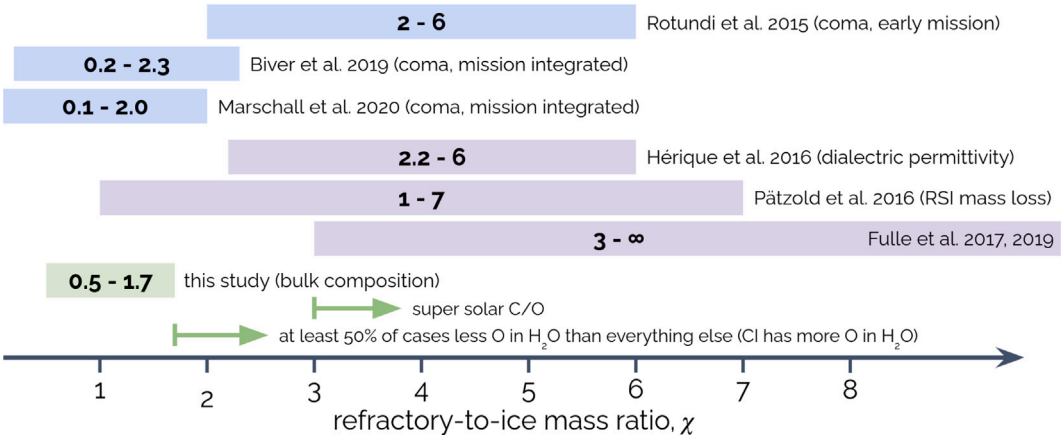

Fig. 7. Summary of literature values for the refractory-to-ice mass ratio, χ: Measurements in the coma are shown in blue and include the ones derived early in the mission from the GIADA instrument (Rotundi et al., 2015), integrated values combining coma gas/dust measurements and the total mass loss (Biver et al., 2019; Marschall et al., 2020b). Estimates from nucleus measurements are shown in purple (Herique et al., 2016; Pätzold et al., 2016; Fulle et al., 2017, 2019). The value we constrain here purely from the elemental composition is shown in green. Additionally, we show the values of χ for which the C/O ratio becomes super solar and the value of χ when at least 50% of cases have less oxygen in water than anything else.

Table 1
The COSIMA elemental abundances (Bardyn et al., 2017) with respect to Iron as well as the derived μ and σ of the log-normal distribution used to model the data.

Z	Element	Name	X/Fe	−	+	μ	σ
1	H	Hydrogen	19.76	15.36	33.04	2.98	0.96
6	C	Carbon	19	14	25	2.94	0.85
7	N	Nitrogen	0.66	0.69	1.1	−0.42	1.02
8	O	Oxygen	19	11	22	2.94	0.75
11	Na	Sodium	0.28	0.18	0.56	−1.27	1.01
12	Mg	Magnesium	0.4	0.2	0.4	−0.92	0.67
13	Al	Aluminum	0.061	0.037	0.095	−2.80	0.88
14	Si	Silicon	3.5	1.7	3.7	1.25	0.68
16	S	Sulfur	0.5	0.094	0.116	−0.69	0.21
19	K	Potassium	0.0074	0.0035	0.0069	−4.91	0.63
20	Ca	Calcium	0.019	0.008	0.015	−3.96	0.56
24	Cr	Chromium	0.0093	0.0035	0.0062	−4.68	0.49
25	Mn	Manganese	0.015	0.003	0.003	−4.20	0.20
26	Fe	Iron	1	0	0	0.00	0.00

χ, xenon is present in quasi-solar abundance. At the same time, krypton is slightly depleted relative to the solar value, and argon is heavily depleted. This pattern naturally occurs if 67P formed from pebbles that were trapped and retained in the 25–35 au region for millions of years. Over this retention time, diffusion causes the volatiles to reach the surface and sublimate if the temperature is high enough. Xenon was thus accreted in the solid form and, therefore, in solar abundance. In contrast, krypton was partially lost, and argon only accreted through adsorption from the gas.

CRediT authorship contribution statement

Raphael Marschall: Writing – original draft, Visualization, Software, Methodology, Investigation, Formal analysis, Conceptualization. **Alessandro Morbidelli:** Writing – original draft, Project administration, Methodology, Investigation, Funding acquisition, Conceptualization. **Yves Marrocchi:** Writing – original draft, Validation, Methodology, Conceptualization.

Declaration of competing interest

The authors declare that they have no known competing financial interests or personal relationships that could have appeared to influence the work reported in this paper.

Acknowledgments

We acknowledge the funding from the European Research Council (ERC) under the European Union's Horizon 2020 research and innovation programme (Grant Agreement No. 101019380). Additionally, we acknowledge support from programme ANR-20-CE49-0006 (ANR DISKBUILD). We thank Martin Rubin for clarifying discussions about their work (Rubin et al., 2019) from which we used the elemental abundances derived from ROSINA data. We thank Nicolas Fray, Anaïs Bardyn, Hervé Cottin, and Martin Hilchenbach for similar clarifying discussions about the most up-to-date COSIMA data to use for the elemental composition of the refractories (Bardyn et al., 2017; Fray et al., 2017). Furthermore, we thank Niels Ligterink for insightful discussions on ad-/desorption and diffusion of noble gases.

Declaration of competing interest

The authors declare that they have no known competing financial interests or personal relationships that could have appeared to influence the work reported in this paper.

Appendix A. Elemental abundances of COSIMA and ROSINA

Each element is assumed to follow a log-normal distribution

$$\frac{1}{x\sigma\sqrt{2\pi}}\exp\left(-\frac{(\ln x-\mu)^2}{2\sigma^2}\right) .$$

The values of μ and σ are shown in Tables 1 and 2, and the comparison of the 'model' to the measurements is shown in Fig. 6.

Appendix B. Bulk elemental abundances of 67P

See Tables 3 and 4.

Appendix C. Using CI composition for the refractory component

One might imagine that instead of the COSIMA measurements, one could use the composition of CI chondrites for the refractory component. If one were to do that, how would our results change?

Table 2
The ROSINA elemental abundances (Rubin et al., 2019) with respect to water as well as the derived μ and σ of the log-normal distribution used to model the data.

Z	Element	Name	X/H_2O	−	+	μ	σ
1	H	Hydrogen	2.1002E+00	3.1708E−02	3.4491E−02	0.74	0.02
6	C	Carbon	9.8983E−02	2.9185E−02	3.0450E−02	−2.31	0.29
7	N	Nitrogen	9.3630E−03	2.8593E−03	2.8593E−03	−4.67	0.30
8	O	Oxygen	1.1980E+00	6.3501E−02	6.9131E−02	0.18	0.06
16	S	Sulfur	1.8557E−02	9.7949E−03	1.4148E−02	−3.99	0.59
18	Ar	Argon	5.8000E−06	2.2000E−06	2.2000E−06	−12.06	0.37
36	Kr	Krypton	4.9000E−07	2.2000E−07	2.2000E−07	−14.53	0.43
54	Xe	Xenon	2.4000E−07	1.1000E−07	1.1000E−07	−15.24	0.44

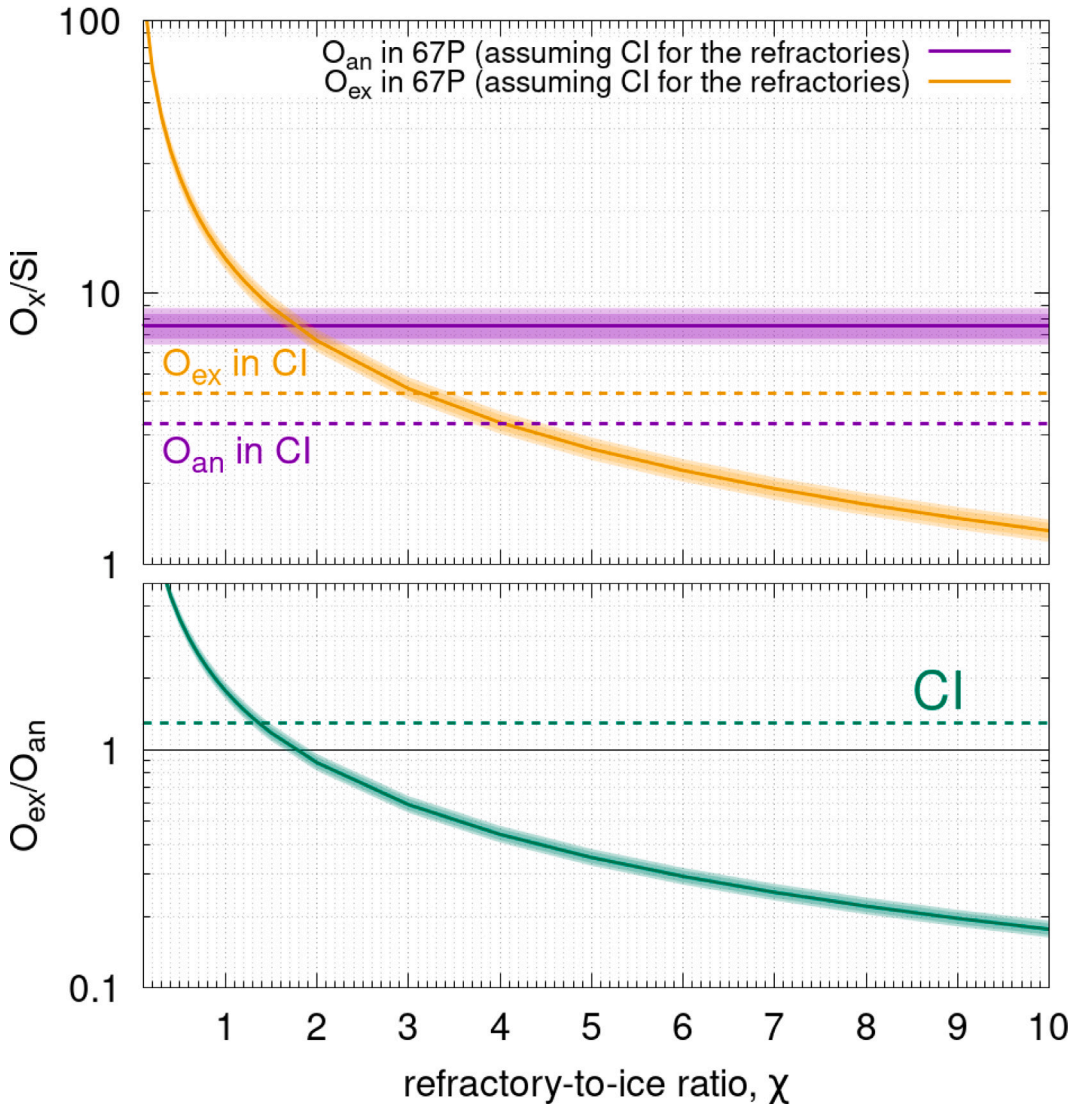

Fig. 8. The top panel shows the oxygen-to-silicon ratio for oxygen that is in water (subscript 'ex') and that which is in anhydrous form (subscript 'an'). Compared to Fig. 2 we assume CI composition for the refractory component of 67P. The values for CI chondrites are taken from Alexander (2019). The bottom panel shows the ratio of the two oxygen components. Note that the bottom panel is not simply the ratio of the lines in the top panel. O_{ex} and O_{an} are not uncorrelated, and therefore, their ratio and respective errors need to be computed for each random draw. The darker shaded areas contain 50% of the cases while the lighter areas contain $\pm 1\sigma$.

If we replace the values used from COSIMA (Table 1) with CI composition, the constraint on the refractory-to-ice ratio becomes $0.35 < \chi < 1.35$, which is very similar to what we find using the COSIMA composition ($0.5 < \chi < 1.7$). Fig. 8 is equivalent to Fig. 2 that we used to constrain the upper limit for χ. For this range ($0.35 < \chi < 1.35$), xenon is solar when $0.35 < \chi < 0.9$. At the upper bound, when $\chi = 1.35$, xenon is slightly sub-solar by 30%. Therefore, even if comet 67P were composed of refractories with CI composition, all our conclusions hold.

Table 3
Bulk elemental abundances of 67P with respect to silicon for the refractory-to-ice mass ratio, $\chi = 0.3$ and 0.5. The errors are $\pm$ 1σ.

Z	Element	Name	$\chi = 0.3$			$\chi = 0.5$		
			X/Si	+	−	X/Si	+	−
1	H	Hydrogen	8.2689E+01	9.5216E+01	4.1470E+01	5.2849E+01	6.1041E+01	2.6713E+01
6	C	Carbon	9.2908E+00	1.4429E+01	5.3951E+00	7.7621E+00	1.2871E+01	4.6455E+00
7	N	Nitrogen	5.8488E−01	7.9705E−01	3.1997E−01	4.3520E−01	6.4395E−01	2.4500E−01
8	O	Oxygen	4.8396E+01	5.8151E+01	2.4576E+01	3.1377E+01	3.8295E+01	1.6105E+01
11	Na	Sodium	7.9736E−02	1.8869E−01	5.6142E−02	7.9736E−02	1.8869E−01	5.6142E−02
12	Mg	Magnesium	1.1364E−01	1.8106E−01	6.9558E−02	1.1364E−01	1.8106E−01	6.9558E−02
13	Al	Aluminum	1.7209E−02	3.4748E−02	1.1480E−02	1.7209E−02	3.4748E−02	1.1480E−02
14	Si	Silicon	1.0000E+00	0.0000E+00	0.0000E+00	1.0000E+00	0.0000E+00	0.0000E+00
16	S	Sulfur	8.2997E−01	1.1444E+00	4.5791E−01	5.6403E−01	7.3344E−01	3.0396E−01
19	K	Potassium	2.1090E−03	3.1999E−03	1.2671E−03	2.1090E−03	3.1999E−03	1.2671E−03
18	Ar	Argon	2.0555E−04	2.7418E−04	1.1058E−04	1.2333E−04	1.6451E−04	6.6349E−05
20	Ca	Calcium	5.4035E−03	7.6795E−03	3.1547E−03	5.4035E−03	7.6795E−03	3.1547E−03
24	Cr	Chromium	2.6481E−03	3.4905E−03	1.5036E−03	2.6481E−03	3.4905E−03	1.5036E−03
25	Mn	Manganese	4.2759E−03	4.3790E−03	2.1680E−03	4.2759E−03	4.3790E−03	2.1680E−03
26	Fe	Iron	2.8590E−01	2.7567E−01	1.4117E−01	2.8590E−01	2.7567E−01	1.4117E−01
36	Kr	Krypton	1.7435E−05	2.4472E−05	9.6898E−06	1.0461E−05	1.4683E−05	5.8139E−06
54	Xe	Xenon	8.5395E−06	1.1927E−05	4.7560E−06	5.1237E−06	7.1563E−06	2.8536E−06

Table 4
Continuation of Table 3 with the bulk elemental abundances of 67P with respect to silicon for the refractory-to-ice mass ratio, χ, of 1.1 and 1.7. The errors are $\pm$ 1σ.

Z	Element	Name	$\chi = 1.1$			$\chi = 1.7$		
			X/Si	+	−	X/Si	+	−
1	H	Hydrogen	2.7996E+01	3.3598E+01	1.4465E+01	2.0543E+01	2.5603E+01	1.0819E+01
6	C	Carbon	6.4843E+00	1.1635E+01	4.0489E+00	6.1019E+00	1.1317E+01	3.8755E+00
7	N	Nitrogen	3.0525E−01	5.2457E−01	1.8182E−01	2.6449E−01	4.9492E−01	1.6259E−01
8	O	Oxygen	1.7401E+01	2.2356E+01	9.1901E+00	1.3257E+01	1.7670E+01	7.1568E+00
11	Na	Sodium	7.9736E−02	1.8869E−01	5.6142E−02	7.9736E−02	1.8869E−01	5.6142E−02
12	Mg	Magnesium	1.1364E−01	1.8106E−01	6.9558E−02	1.1364E−01	1.8106E−01	6.9558E−02
13	Al	Aluminum	1.7209E−02	3.4748E−02	1.1480E−02	1.7209E−02	3.4748E−02	1.1480E−02
14	Si	Silicon	1.0000E+00	0.0000E+00	0.0000E+00	1.0000E+00	0.0000E+00	0.0000E+00
16	S	Sulfur	3.4247E−01	4.0175E−01	1.7770E−01	2.7567E−01	3.0737E−01	1.4067E−01
19	K	Potassium	2.1090E−03	3.1999E−03	1.2671E−03	2.1090E−03	3.1999E−03	1.2671E−03
18	Ar	Argon	5.6059E−05	7.4775E−05	3.0159E−05	3.6273E−05	4.8384E−05	1.9514E−05
20	Ca	Calcium	5.4035E−03	7.6795E−03	3.1547E−03	5.4035E−03	7.6795E−03	3.1547E−03
24	Cr	Chromium	2.6481E−03	3.4905E−03	1.5036E−03	2.6481E−03	3.4905E−03	1.5036E−03
25	Mn	Manganese	4.2759E−03	4.3790E−03	2.1680E−03	4.2759E−03	4.3790E−03	2.1680E−03
26	Fe	Iron	2.8590E−01	2.7567E−01	1.4117E−01	2.8590E−01	2.7567E−01	1.4117E−01
36	Kr	Krypton	4.7550E−06	6.6742E−06	2.6427E−06	3.0767E−06	4.3186E−06	1.7100E−06
54	Xe	Xenon	2.3289E−06	3.2529E−06	1.2971E−06	1.5070E−06	2.1048E−06	8.3929E−07

Data availability

All data used is included in the paper and appendix.

References

A'Hearn, M.F., Belton, M.J.S., Delamere, A., Blume, W.H., 2005. Deep impact: A large-scale active experiment on a cometary nucleus. Space Sci. Rev. 117 (1–2), 1–21. http://dx.doi.org/10.1007/s11214-005-3387-3.

A'Hearn, M.F., Belton, M.J.S., Delamere, W.A., Feaga, L.M., Hampton, D., Kissel, J., Klaasen, K.P., McFadden, L.A., Meech, K.J., Melosh, H.J., Schultz, P.H., Sunshine, J.M., Thomas, P.C., Veverka, J., Wellnitz, D.D., Yeomans, D.K., Besse, S., Bodewits, D., Bowling, T.J., Carcich, B.T., Collins, S.M., Farnham, T.L., Groussin, O., Hermalyn, B., Kelley, M.S., Kelley, M.S., Li, J.-Y., Lindler, D.J., Lisse, C.M., McLaughlin, S.A., Merlin, F., Protopapa, S., Richardson, J.E., Williams, J.L., 2011. EPOXI at comet hartley 2. Science 332 (6036), 1396. http://dx.doi.org/10.1126/science.1204054.

Alexander, C.M.O., 2019. Quantitative models for the elemental and isotopic fractionations in chondrites: The carbonaceous chondrites. Geochim. Cosmochimica Acta 254, 277–309. http://dx.doi.org/10.1016/j.gca.2019.02.008.

Alexander, C.M.O.D., Fogel, M., Yabuta, H., Cody, G.D., 2007. The origin and evolution of chondrites recorded in the elemental and isotopic compositions of their macromolecular organic matter. Geochim. Cosmochimica Acta 71 (17), 4380–4403. http://dx.doi.org/10.1016/j.gca.2007.06.052.

Amelin, Y., Kaltenbach, A., Iizuka, T., Stirling, C.H., Ireland, T.R., Petaev, M., Jacobsen, S.B., 2010. U-Pb chronology of the solar system's oldest solids with variable ^{238}U/ ^{235}U. Earth Planet. Sci. Lett. 300 (3–4), 343–350. http://dx.doi.org/10.1016/j.epsl.2010.10.015.

Andrews, S.M., 2020. Observations of protoplanetary disk structures. Annu. Rev. Astron. Astrophys. 58, 483–528. http://dx.doi.org/10.1146/annurev-astro-031220-010302, arXiv:2001.05007.

Appelgren, J., Lambrechts, M., Johansen, A., 2020. Dust clearing by radial drift in evolving protoplanetary discs. Astron. Astrophys. 638, A156. http://dx.doi.org/10.1051/0004-6361/202037650, arXiv:2004.02918.

Asplund, M., Amarsi, A.M., Grevesse, N., 2021. The chemical make-up of the sun: A 2020 vision. Astron. Astrophys. 653, A141. http://dx.doi.org/10.1051/0004-6361/202140445, arXiv:2105.01661.

Balsiger, H., Altwegg, K., Bar-Nun, A., Berthelier, J.-J., Bieler, A., Bochsler, P., Briois, C., Calmonte, U., Combi, M., Keyser, J.D., Eberhardt, P., Fiethe, B., Fuselier, S.A., Gasc, S., Gombosi, T.I., Hansen, K.C., Hässig, M., Jäckel, A., Kopp, E., Korth, A., Roy, L.L., Mall, U., Marty, B., Mousis, O., Owen, T., Rème, H., Rubin, M., Sémon, T., Tzou, C.-Y., Waite, J.H., Wurz, P., 2015. Detection of argon in the coma of comet 67P/Churyumov-Gerasimenko. Sci. Adv. 1 (8), e1500377. http://dx.doi.org/10.1126/sciadv.1500377, arXiv:https://www.science.org/doi/pdf/10.1126/sciadv.1500377 URL https://www.science.org/doi/abs/10.1126/sciadv.1500377.

Balsiger, H., Altwegg, K., Bochsler, P., Eberhardt, P., Fischer, J., Graf, S., Jäckel, A., Kopp, E., Langer, U., Mildner, M., Müller, J., Riesen, T., Rubin, M., Scherer, S., Wurz, P., Wüthrich, S., Arijs, E., Delanoye, S., de Keyser, J., Neefs, E., Nevejans, D., Rème, H., Aoustin, C., Mazelle, C., Médale, J.L., Sauvaud, J.A., Berthelier, J.J., Bertaux, J.L., Duvet, L., Illiano, J.M., Fuselier, S.A., Ghielmetti, A.G., Magoncelli, T.,

Shelley, E.G., Korth, A., Heerlein, K., Lauche, H., Livi, S., Loose, A., Mall, U., Wilken, B., Gliem, F., Fiethe, B., Gombosi, T.I., Block, B., Carignan, G.R., Fisk, L.A., Waite, J.H., Young, D.T., Wollnik, H., 2007. Rosina Rosetta orbiter spectrometer for ion and neutral analysis. Space Sci. Rev. 128 (1–4), 745–801. http://dx.doi.org/10.1007/s11214-006-8335-3.

Bardyn, A., Baklouti, D., Cottin, H., Fray, N., Briois, C., Paquette, J., Stenzel, O., Engrand, C., Fischer, H., Hornung, K., Isnard, R., Langevin, Y., Lehto, H., Le Roy, L., Ligier, N., Merouane, S., Modica, P., Orthous-Daunay, F.-R., Rynö, J., Schulz, R., Silén, J., Thirkell, L., Varmuza, K., Zaprudin, B., Kissel, J., Hilchenbach, M., 2017. Carbon-rich dust in comet 67p/Churyumov-Gerasimenko measured by COSIMA/Rosetta. Mon. Not. R. Astron. Soc. 469, S712–S722. http://dx.doi.org/10.1093/mnras/stx2640.

Berthier, J., Descamps, P., Vachier, F., Normand, J., Maquet, L., Deleflie, F., Colas, F., Klotz, A., Teng-Chuen-Yu, J.P., Peyrot, A., Braga-Ribas, F., Marchis, F., Leroy, A., Bouley, S., Dubos, G., Pollock, J., Pauwels, T., Vingerhoets, P., Farrell, J.A., Sada, P.V., Reddy, V., Archer, K., Hamanowa, H.H., 2020. Physical characterization of double asteroid (617) Patroclus from 2007/2012 mutual events observations. Icarus 352, 113990. http://dx.doi.org/10.1016/j.icarus.2020.113990.

Birnstiel, T., 2024. Dust growth and evolution in protoplanetary disks. Annu. Rev. Astron. Astrophys. 62 (1), 157–202. http://dx.doi.org/10.1146/annurev-astro-071221-052705, arXiv:2312.13287.

Bitsch, B., Battistini, C., 2020. Influence of sub- and super-solar metallicities on the composition of solid planetary building blocks. Astron. Astrophys. 633, A10. http://dx.doi.org/10.1051/0004-6361/201936463, arXiv:1911.09725.

Biver, N., Bockelée-Morvan, D., Colom, P., Crovisier, J., Germain, B., Lellouch, E., Davies, J.K., Dent, W.R.F., Moreno, R., Paubert, G., Wink, J., Despois, D., Lis, D.C., Mehringer, D., Benford, D., Gardner, M., Phillips, T.G., Gunnarsson, M., Rickman, H., Winnberg, A., Bergman, P., Johansson, L.E.B., Rauer, H., 1997. Long-term evolution of the outgassing of Comet Hale-Bopp from radio observations. Earth Moon Planets 78, 5–11. http://dx.doi.org/10.1023/A:1006229818484.

Biver, N., Bockelée-Morvan, D., Hofstadter, M., Lellouch, E., Choukroun, M., Gulkis, S., Crovisier, J., Schloerb, F.P., Rezac, L., von Allmen, P., Lee, S., Leyrat, C., Ip, W.H., Hartogh, P., Encrenaz, P., Beaudin, G., MIRO Team, 2019. Long-term monitoring of the outgassing and composition of comet 67P/Churyumov-Gerasimenko with the Rosetta/MIRO instrument. Astron. Astrophys. 630, A19. http://dx.doi.org/10.1051/0004-6361/201834960.

Bottke, W.F., Vokrouhlický, D., Marschall, R., Nesvorný, D., Morbidelli, A., Deienno, R., Marchi, S., Dones, L., Levison, H.F., 2023. The collisional evolution of the Primordial Kuiper Belt, its destabilized population, and the Trojan Asteroids. Planet. Sci. J. 4 (9), 168. http://dx.doi.org/10.3847/PSJ/ace7cd, arXiv:2307.07089.

Brown, M.E., 2013. The density of mid-sized kuiper belt object 2002 UX25 and the formation of the Dwarf Planets. Astrophys. J. Lett. 778 (2), L34. http://dx.doi.org/10.1088/2041-8205/778/2/L34, arXiv:1311.0553.

Chiang, E., Youdin, A.N., 2010. Forming planetesimals in solar and extrasolar nebulae. Annu. Rev. Earth Planet. Sci. 38, 493–522. http://dx.doi.org/10.1146/annurev-earth-040809-152513, arXiv:0909.2652.

Choukroun, M., Altwegg, K., Kührt, E., Biver, N., Bockelée-Morvan, D., Drążkowska, J., Hérique, A., Hilchenbach, M., Marschall, R., Pätzold, M., Taylor, M.G.G.T., Thomas, N., 2020. Dust-to-gas and refractory-to-ice mass ratios of Comet 67P/Churyumov-Gerasimenko from Rosetta Observations. Space Sci. Rev. 216 (3), 44. http://dx.doi.org/10.1007/s11214-020-00662-1.

Combi, M., Shou, Y., Fougere, N., Tenishev, V., Altwegg, K., Rubin, M., Bockelée-Morvan, D., Capaccioni, F., Cheng, Y.-C., Fink, U., Gombosi, T., Hansen, K.C., Huang, Z., Marshall, D., Toth, G., 2020. The surface distributions of the production of the major volatile species, H_2O, CO_2, CO and O_2, from the nucleus of comet 67P/Churyumov-Gerasimenko throughout the Rosetta Mission as measured by the ROSINA double focusing mass spectrometer. Icarus 335, 113421. http://dx.doi.org/10.1016/j.icarus.2019.113421, arXiv:1909.02082.

Connelly, J.N., Bizzarro, M., Krot, A.N., Nordlund, Å., Wielandt, D., Ivanova, M.A., 2012. The absolute chronology and thermal processing of solids in the solar protoplanetary disk. Science 338 (6107), 651. http://dx.doi.org/10.1126/science.1226919.

Davidsson, B.J.R., Birch, S., Blake, G.A., Bodewits, D., Dworkin, J.P., Glavin, D.P., Furukawa, Y., Lunine, J.I., Mitchell, J.L., Nguyen, A.N., Squyres, S., Takigawa, A., Vincent, J.-B., Zacny, K., 2021. Airfall on comet 67p/Churyumov-Gerasimenko. Icarus 354, 114004. http://dx.doi.org/10.1016/j.icarus.2020.114004, arXiv:2208.01089.

Dones, L., Brasser, R., Kaib, N., Rickman, H., 2015. Origin and evolution of the cometary reservoirs. Space Sci. Rev. 197 (1–4), 191–269. http://dx.doi.org/10.1007/s11214-015-0223-2.

Drążkowska, J., Dullemond, C.P., 2018. Planetesimal formation during protoplanetary disk buildup. Astron. Astrophys. 614, A62. http://dx.doi.org/10.1051/0004-6361/201732221, arXiv:1803.00575.

Duncan, M.J., 2008. Dynamical origin of comets and their reservoirs. Space Sci. Rev. 138 (1–4), 109–126. http://dx.doi.org/10.1007/s11214-008-9405-5.

Duncan, M., Levison, H., Dones, L., 2004. Dynamical evolution of ecliptic comets. In: Festou, M.C., Keller, H.U., Weaver, H.A. (Eds.), Comets II. p. 193.

Eberhardt, P., Krankowsky, D., Schulte, W., Dolder, U., Lammerzahl, P., Berthelier, J.J., Woweries, J., Stubbemann, U., Hodges, R.R., Hoffman, J.H., Illiano, J.M., 1987. To CO and n_2 abundance in Comet p/ Halley. Astron. Astrophys. 187, 481.

Fray, N., Bardyn, A., Cottin, H., Altwegg, K., Baklouti, D., Briois, C., Colangeli, L., Engrand, C., Fischer, H., Glasmachers, A., Grün, E., Haerendel, G., Henkel, H., Höfner, H., Hornung, K., Jessberger, E.K., Koch, A., Krüger, H., Langevin, Y., Lehto, H., Lehto, K., Le Roy, L., Merouane, S., Modica, P., Orthous-Daunay, F.-R., Paquette, J., Raulin, F., Rynö, J., Schulz, R., Silén, J., Siljeström, S., Steiger, W., Stenzel, O., Stephan, T., Thirkell, L., Thomas, R., Torkar, K., Varmuza, K., Wanczek, K.-P., Zaprudin, B., Kissel, J., Hilchenbach, M., 2016. High-molecular-weight organic matter in the particles of comet 67P/Churyumov-Gerasimenko. Nature 538 (7623), 72–74. http://dx.doi.org/10.1038/nature19320.

Fray, N., Bardyn, A., Cottin, H., Baklouti, D., Briois, C., Engrand, C., Fischer, H., Hornung, K., Isnard, R., Langevin, Y., Lehto, H., Le Roy, L., Mellado, E.M., Merouane, S., Modica, P., Orthous-Daunay, F.-R., Paquette, J., Rynö, J., Schulz, R., Silén, J., Siljeström, S., Stenzel, O., Thirkell, L., Varmuza, K., Zaprudin, B., Kissel, J., Hilchenbach, M., 2017. Nitrogen-to-carbon atomic ratio measured by COSIMA in the particles of comet 67P/Churyumov-Gerasimenko. Mon. Not. R. Astron. Soc. 469, S506–S516. http://dx.doi.org/10.1093/mnras/stx2002.

Fulle, M., Blum, J., Green, S.F., Gundlach, B., Herique, A., Moreno, F., Mottola, S., Rotundi, A., Snodgrass, C., 2019. The refractory-to-ice mass ratio in comets. Mon. Not. R. Astron. Soc. 482 (3), 3326–3340. http://dx.doi.org/10.1093/mnras/sty2926.

Fulle, M., Della Corte, V., Rotundi, A., Green, S.F., Accolla, M., Colangeli, L., Ferrari, M., Ivanovski, S., Sordini, R., Zakharov, V., 2017. The dust-to-ices ratio in comets and Kuiper belt objects. Mon. Not. R. Astron. Soc. 469, S45–S49. http://dx.doi.org/10.1093/mnras/stx983.

Gasc, S., Altwegg, K., Balsiger, H., Berthelier, J.-J., Bieler, A., Calmonte, U., Fiethe, B., Fuselier, S., Galli, A., Gombosi, T., Hoang, M., De Keyser, J., Korth, A., Le Roy, L., Mall, U., Rème, H., Rubin, M., Sémon, T., Tzou, C.-Y., Waite, J.H., Wurz, P., 2017. Change of outgassing pattern of 67P/Churyumov-Gerasimenko during the March 2016 equinox as seen by ROSINA. Mon. Not. R. Astron. Soc. 469, S108–S117. http://dx.doi.org/10.1093/mnras/stx1412.

Gkotsinas, A., Nesvorný, D., Guilbert-Lepoutre, A., Raymond, S.N., Kaib, N., 2024. On the early thermal processing of planetesimals during and after the giant planet instability. Planet. Sci. J. 5 (11), 243. http://dx.doi.org/10.3847/PSJ/ad7f4e, arXiv:2410.01923.

Groussin, O., Attree, N., Brouet, Y., Ciarletti, V., Davidsson, B., Filacchione, G., Fischer, H.-H., Gundlach, B., Knapmeyer, M., Knollenberg, J., Kokotanekova, R., Kührt, E., Leyrat, C., Marshall, D., Pelivan, I., Skorov, Y., Snodgrass, C., Spohn, T., Tosi, F., 2019. The thermal, mechanical, structural, and dielectric properties of cometary nuclei after rosetta. Space Sci. Rev. 215 (4), 29. http://dx.doi.org/10.1007/s11214-019-0594-x.

Guilbert-Lepoutre, A., Rosenberg, E.D., Prialnik, D., Besse, S., 2016. Modelling the evolution of a comet subsurface: implications for 67P/Churyumov-Gerasimenko. Mon. Not. R. Astron. Soc. 462, S146–S155. http://dx.doi.org/10.1093/mnras/stw2371.

Herique, A., Kofman, W., Beck, P., Bonal, L., Buttarazzi, I., Heggy, E., Lasue, J., Levasseur-Regourd, A.C., Quirico, E., Zine, S., 2016. Cosmochemical implications of CONSERT permittivity characterization of 67P/CG. Mon. Not. R. Astron. Soc. 462, S516–S532. http://dx.doi.org/10.1093/mnras/stx040.

Isnard, R., Bardyn, A., Fray, N., Briois, C., Cottin, H., Paquette, J., Stenzel, O., Alexander, C., Baklouti, D., Engrand, C., Orthous-Daunay, F.R., Siljeström, S., Varmuza, K., Hilchenbach, M., 2019. H/C elemental ratio of the refractory organic matter in cometary particles of 67P/Churyumov-Gerasimenko. Astron. Astrophys. 630, A27. http://dx.doi.org/10.1051/0004-6361/201834797.

Jutzi, M., Michel, P., 2020. Collisional heating and compaction of small bodies: Constraints for their origin and evolution. Icarus 350, 113867. http://dx.doi.org/10.1016/j.icarus.2020.113867, arXiv:2005.12785.

Keller, H.U., Kührt, E., 2020. Cometary nuclei—from Giotto to Rosetta. Space Sci. Rev. 216 (1), 14. http://dx.doi.org/10.1007/s11214-020-0634-6.

Kelley, M.S.P., Kokotanekova, R., Holt, C.E., Protopapa, S., Bodewits, D., Knight, M.M., Lister, T., Usher, H., Chatelain, J., Gomez, E., Greenstreet, S., Angel, T., Wooding, B., 2022. A look at outbursts of Comet C/2014 UN_{271} (Bernardinelli-Bernstein) near 20 au. Astrophys. J. Lett. 933 (2), L44. http://dx.doi.org/10.3847/2041-8213/ac7bec, arXiv:2206.14888.

Kissel, J., Altwegg, K., Clark, B.C., Colangeli, L., Cottin, H., Czempiel, S., Eibl, J., Engrand, C., Fehringer, H.M., Feuerbacher, B., Fomenkova, M., Glasmachers, A., Greenberg, J.M., Grün, E., Haerendel, G., Henkel, H., Hilchenbach, M., von Hoerner, H., Höfner, H., Hornung, K., Jessberger, E.K., Koch, A., Krüger, H., Langevin, Y., Parigger, P., Raulin, F., Rüdenauer, F., Rynö, J., Schmid, E.R., Schulz, R., Silén, J., Steiger, W., Stephan, T., Thirkell, L., Thomas, R., Torkar, K., Utterback, N.G., Varmuza, K., Wanczek, K.P., Werther, W., Zscheeg, H., 2007. Cosima high resolution time-of-flight secondary ion mass spectrometer for the

analysis of cometary dust particles onboard rosetta. Space Sci. Rev. 128 (1–4), 823–867. http://dx.doi.org/10.1007/s11214-006-9083-0.

Läuter, M., Kramer, T., Rubin, M., Altwegg, K., 2020. The gas production of 14 species from comet 67P/Churyumov-Gerasimenko based on DFMS/COPS data from 2014 to 2016. Mon. Not. R. Astron. Soc. 498 (3), 3995–4004. http://dx.doi.org/10.1093/mnras/staa2643.

Ligterink, N.F.W., Kipfer, K.A., Rubin, M., Altwegg, K., Hänni, N., Müller, D.R., Wurz, P., Galli, A., Wampfler, S.F., 2024. Sublimation of volatiles from H_2O:CO_2 bulk ices in the context of comet 67P/Churyumov-Gerasimenko. II. Noble gases. Astron. Astrophys. 687, A78. http://dx.doi.org/10.1051/0004-6361/202449554.

Livingston, F.E., Smith, J.A., George, S.M., 2002. General trends for bulk diffusion in ice and surface diffusion on ice. J. Phys. Chem. A 106 (26), 6309–6318.

Lodders, K., 2003. Solar system abundances and condensation temperatures of the elements. Astrophys. J. 591 (2), 1220–1247. http://dx.doi.org/10.1086/375492.

Marschall, R., Markkanen, J., Gerig, S.-B., Pinzón-Rodríguez, O., Thomas, N., Wu, J.-S., 2020b. The dust-to-gas ratio, size distribution, and dust fall-back fraction of Comet 67P/Churyumov-Gerasimenko: Inferences from linking the optical and dynamical properties of the inner comae. Front. Phys. 8, 227. http://dx.doi.org/10.3389/fphy.2020.00227, URL https://www.frontiersin.org/article/10.3389/fphy.2020.00227.

Marschall, R., Morbidelli, A., 2023. An inflationary disk phase to explain extended protoplanetary dust disks. Astron. Astrophys. 677, A136. http://dx.doi.org/10.1051/0004-6361/202346616, arXiv:2307.01249.

Marty, B., Altwegg, K., Balsiger, H., Bar-Nun, A., Bekaert, D.V., Berthelier, J.J., Bieler, A., Briois, C., Calmonte, U., Combi, M., De Keyser, J., Fiethe, B., Fuselier, S.A., Gasc, S., Gombosi, T.I., Hansen, K.C., Hässig, M., Jäckel, A., Kopp, E., Korth, A., Le Roy, L., Mall, U., Mousis, O., Owen, T., Rème, H., Rubin, M., Sémon, T., Tzou, C.Y., Waite, J.H., Wurz, P., 2017. Xenon isotopes in 67P/Churyumov-Gerasimenko show that comets contributed to Earth's atmosphere. Science 356 (6342), 1069–1072. http://dx.doi.org/10.1126/science.aal3496.

Morbidelli, A., Baillié, K., Batygin, K., Charnoz, S., Guillot, T., Rubie, D.C., Kleine, T., 2022. Contemporary formation of early solar system planetesimals at two distinct radial locations. Nat. Astron. 6, 72–79. http://dx.doi.org/10.1038/s41550-021-01517-7, arXiv:2112.15413.

Najita, J.R., Bergin, E.A., 2018. Protoplanetary disk sizes and angular momentum transport. Astrophys. J. 864 (2), 168. http://dx.doi.org/10.3847/1538-4357/aad80c, arXiv:1808.05618.

Nesvorný, D., 2018. Dynamical evolution of the early solar system. Annu. Rev. Astron. Astrophys. 56, 137–174. http://dx.doi.org/10.1146/annurev-astro-081817-052028, arXiv:1807.06647.

Nesvorný, D., 2021. Eccentric early migration of neptune. Astrophys. J. Lett. 908 (2), L47. http://dx.doi.org/10.3847/2041-8213/abe38f, arXiv:2012.13648.

Nesvorný, D., Vokrouhlický, D., Roig, F., 2016. The orbital distribution of trans-neptunian objects beyond 50 au. Astrophys. J. Lett. 827 (2), L35. http://dx.doi.org/10.3847/2041-8205/827/2/L35, arXiv:1607.08279.

Neumann, W., Kruijer, T.S., Breuer, D., Kleine, T., 2018. Multistage core formation in planetesimals revealed by numerical modeling and Hf-W chronometry of iron meteorites. J. Geophys. Res. (Planets) 123 (2), 421–444. http://dx.doi.org/10.1002/2017JE005411.

Öberg, K.I., Wordsworth, R., 2019. Jupiter's composition suggests its core assembled exterior to the n_2 snowline. Astron. J. 158 (5), 194. http://dx.doi.org/10.3847/1538-3881/ab46a8, arXiv:1909.11246.

Pätzold, M., Andert, T., Hahn, M., Asmar, S.W., Barriot, J.P., Bird, M.K., Häusler, B., Peter, K., Tellmann, S., Grün, E., Weissman, P.R., Sierks, H., Jorda, L., Gaskell, R., Preusker, F., Scholten, F., 2016. A homogeneous nucleus for comet 67P/Churyumov-Gerasimenko from its gravity field. Nature 530 (7588), 63–65. http://dx.doi.org/10.1038/nature16535.

Rayman, M.D., 2002. The Deep Space 1 extended mission: Challenges in preparing for an encounter with comet borrelly. Acta Astronaut. 51 (1), 507–516. http://dx.doi.org/10.1016/S0094-5765(02)00070-X.

Raymond, S.N., Izidoro, A., 2017. Origin of water in the inner solar system: Planetesimals scattered inward during Jupiter and Saturn's rapid gas accretion. Icarus 297, 134–148. http://dx.doi.org/10.1016/j.icarus.2017.06.030, arXiv:1707.01234.

Reichhardt, T., 1995. Stardust mission will collect Comet dust. Nature 378, 527.

Rotundi, A., Sierks, H., Della Corte, V., Fulle, M., Gutierrez, P.J., Lara, L., Barbieri, C., Lamy, P.L., Rodrigo, R., Koschny, D., Rickman, H., Keller, H.U., López-Moreno, J.J., Accolla, M., Agarwal, J., A'Hearn, M.F., Altobelli, N., Angrilli, F., Barucci, M.A., Bertaux, J.-L., Bertini, I., Bodewits, D., Bussoletti, E., Colangeli, L., Cosi, M., Cremonese, G., Crifo, J.-F., Da Deppo, V., Davidsson, B., Debei, S., De Cecco, M., Esposito, F., Ferrari, M., Fornasier, S., Giovane, F., Gustafson, B., Green, S.F., Groussin, O., Grün, E., Güttler, C., Herranz, M.L., Hviid, S.F., Ip, W., Ivanovski, S., Jerónimo, J.M., Jorda, L., Knollenberg, J., Kramm, R., Kührt, E., Küppers, M., Lazzarin, M., Leese, M.R., López-Jiménez, A.C., Lucarelli, F., Lowry, S.C., Marzari, F., Epifani, E.M., McDonnell, J.A.M., Mennella, V., Michalik, H., Molina, A., Morales, R., Moreno, F., Mottola, S., Naletto, G., Oklay, N., Ortiz, J.L., Palomba, E., Palumbo, P., Perrin, J.-M., Rodríguez, J., Sabau, L., Snodgrass, C., Sordini, R., Thomas, N., Tubiana, C., Vincent, J.-B., Weissman, P., Wenzel, K.-P., Zakharov, V., Zarnecki, J.C., 2015. Dust measurements in the coma of comet 67P/Churyumov-Gerasimenko inbound to the Sun. Science 347 (6220), aaa3905. http://dx.doi.org/10.1126/science.aaa3905.

Rubin, M., Altwegg, K., Balsiger, H., Berthelier, J.-J., Combi, M.R., De Keyser, J., Drozdovskaya, M., Fiethe, B., Fuselier, S.A., Gasc, S., Gombosi, T.I., Hänni, N., Hansen, K.C., Mall, U., Rème, H., Schroeder, I.R.H.G., Schuhmann, M., Sémon, T., Waite, J.H., Wampfler, S.F., Wurz, P., 2019. Elemental and molecular abundances in comet 67P/Churyumov-Gerasimenko. Mon. Not. R. Astron. Soc. 489 (1), 594–607. http://dx.doi.org/10.1093/mnras/stz2086, arXiv:1907.11044.

Smith, R.S., Huang, C., Kay, B.D., 1997. Evidence for molecular translational diffusion during the crystallization of amorphous solid water. J. Phys. Chem. B 101 (32), 6123–6126.

Snodgrass, C., Fitzsimmons, A., Lowry, S.C., Weissman, P., 2011. The size distribution of Jupiter Family comet nuclei. Mon. Not. R. Astron. Soc. 414 (1), 458–469. http://dx.doi.org/10.1111/j.1365-2966.2011.18406.x, arXiv:1101.4228.

Spencer, J.R., Stern, S.A., Moore, J.M., Weaver, H.A., Singer, K.N., Olkin, C.B., Verbiscer, A.J., McKinnon, W.B., Parker, J.W., Beyer, R.A., Keane, J.T., Lauer, T.R., Porter, S.B., White, O.L., Buratti, B.J., El-Maarry, M.R., Lisse, C.M., Parker, A.H., Throop, H.B., Robbins, S.J., Umurhan, O.M., Binzel, R.P., Britt, D.T., Buie, M.W., Cheng, A.F., Cruikshank, D.P., Elliott, H.A., Gladstone, G.R., Grundy, W.M., Hill, M.E., Horanyi, M., Jennings, D.E., Kavelaars, J.J., Linscott, I.R., McComas, D.J., McNutt, R.L., Protopapa, S., Reuter, D.C., Schenk, P.M., Showalter, M.R., Young, L.A., Zangari, A.M., Abedin, A.Y., Beddingfield, C.B., Benecchi, S.D., Bernardoni, E., Bierson, C.J., Borncamp, D., Bray, V.J., Chaikin, A.L., Dhingra, R.D., Fuentes, C., Fuse, T., Gay, P.L., Gwyn, S.D.J., Hamilton, D.P., Hofgartner, J.D., Holman, M.J., Howard, A.D., Howett, C.J.A., Karoji, H., Kaufmann, D.E., Kinczyk, M., May, B.H., Mountain, M., Pätzold, M., Petit, J.M., Piquette, M.R., Reid, I.N., Reitsema, H.J., Runyon, K.D., Sheppard, S.S., Stansberry, J.A., Stryk, T., Tanga, P., Tholen, D.J., Trilling, D.E., Wasserman, L.H., 2020. The geology and geophysics of Kuiper Belt object (486958) Arrokoth. Science 367 (6481), aay3999. http://dx.doi.org/10.1126/science.aay3999, arXiv:2004.00727.

Takeuchi, T., Lin, D.N.C., 2002. Radial flow of dust particles in accretion disks. Astrophys. J. 581 (2), 1344–1355. http://dx.doi.org/10.1086/344437, arXiv:astro-ph/0208552.

Takeuchi, T., Lin, D.N.C., 2005. Attenuation of millimeter emission from circumstellar disks induced by the rapid dust accretion. Astrophys. J. 623 (1), 482–492. http://dx.doi.org/10.1086/428378, arXiv:astro-ph/0410095.

Taylor, M.G.G.T., Altobelli, N., Buratti, B.J., Choukroun, M., 2017. The Rosetta mission orbiter science overview: the comet phase. Philos. Trans. R. Soc. Lond. Ser. A 375 (2097), 20160262. http://dx.doi.org/10.1098/rsta.2016.0262, arXiv:1703.10462.

Weissman, P., Morbidelli, A., Davidsson, B., Blum, J., 2020. Origin and evolution of cometary nuclei. Space Sci. Rev. 216 (1), 6. http://dx.doi.org/10.1007/s11214-019-0625-7.

Yokochi, R., 2022. Adsorption-driven gas trapping in cometary ice analogs. Astrophys. J. 940 (2), 153. http://dx.doi.org/10.3847/1538-4357/ac9621.